Modeling sub-grid scale mixing of vapor in diesel sprays using jet theory

Neerav Abani* and Rolf D. Reitz
Engine Research Center, Department of Mechanical Engineering,
University of Wisconsin-Madison
Madison, WI 53705 USA

Abstract

In a reacting diesel spray the flame stabilizes at the lift-off location. It is widely known that mixing in reacting sprays is an important factor in the determination of the lift-off length. These details can be captured using computational techniques using CFD with a very fine mesh resolution. Use of a coarse resolution over-predicts mixing due to large numerical diffusion and thus reduces the lift-off length. In this study a sub-grid scale model based on classical jet theory is presented, where the vapor-air mixing is modeled with a combined Lagrangian and Eulerian approach. The vapor is transported as a Lagrangian particle consistent with jet mixing and transport theory until the jet mixing is resolved by the mesh scale. In this way, the results show improved predictions of lift-off length with coarse mesh resolutions. The new model offers a potential tool for investigating reacting sprays with coarser mesh resolution in order to save computational time.

Introduction

In a reacting spray such as diesel sprays the fuel droplets atomize, entrain and mix with the surrounding air and travel downstream of the injector location to a certain distance before the fuel starts burning. This distance is called the flame lift-off length and represents the start of combustion of the turbulent fuel spray under the given ambient conditions. The flame lift-off length in diesel fuel jets has been investigated experimentally and numerically using computational fluid dynamics (CFD) under quiescent conditions extensively in previous works. Siebers et al. [1,2] and Picket et al. [3] experimentally investigated the effect of various parameters such as injection pressure, ambient temperature, ambient oxygen concentration and the ignition process on the flame lift-off length in an optically-accessible combustion chamber. Vishwanathan and Reitz [4] investigated flame lift-off computationally using the multi-dimensional CFD code KIVA to investigate and validate reacting spray models with experimental results of Picket et al. [3]. These computational models are widely used by researchers as a tool to design and improve engine emissions, fuel consumption and for combustion control [5, 6].

Standard spray models are modeled using the Lagrangian-Drop and Eulerian-Fluid (LDEF) method [7], where the droplets issuing from the nozzle are transported as particles and interact with the surrounding gas by exchanging mass, momentum and energy. Reitz [8] and Patterson et al. [9] enhanced these models by including the effects of droplet breakup. The droplet collisions and coalescences are modeled using O'Rourke's approach [10] that is stochastically based. In the case of engine combustion these models are coupled with detailed chemistry and turbulence models to solve for the chemical reactions. The near-nozzle spray processes of drop breakup, collision and coalescence occur due to near-nozzle turbulent-jet mixing and must be resolved in order to predict accurate flame lift-off lengths.

In recent times advances in computational techniques, computer processor speed and optimization techniques have provided additional tools for research in the area of engine combustion. These tools can provide the best possible solution by optimizing the various parameters effecting engine combustion using Genetic Algorithms (GA) [5, 6]. Advances in computational techniques and processing speed also allow the use of finer meshes for CFD solutions of combustion. But the use of finer meshes for optimizing engine combustion is still computationally very time consuming because of the requirement to investigate numerous permutations and combinations of different engine design parameters. Hence, the use of a coarser mesh is a practical approach for detailed optimization studies.

This fact emphasizes the need for reacting spray models to be mesh (or grid) independent so that a coarse and a fine mesh would provide the same engine combustion solution and emissions, in-cylinder pressure and rate of heat release predictions. Abraham et al. [11] found that spray and gaseous fuel jets need to be resolved to at least the scale of the nozzle diameter for an accurate prediction of spray structure and tip-penetration. Schmidt and Rutland [12] improved upon collision models to reduce grid-dependency. Abani et al. [13] found that LDEF spray models

* Graduate Research Assistant, University of Wisconsin-Madison, abani@wisc.edu

are grid-dependent because of the inability of these models to predict accurately the drop-gas relative velocity at different mesh scales. Using steady-state jet theory they were able to predict accurate relative velocities and were able to obtain accurate and consistent spray structure, penetration and drop size predictions [14, 15]. Abani and Reitz [16] extended the steady-state jet theory to unsteady injections and found that the grid-independent models improved the engine predictions [17]. Beard et al. [18] improved the prediction of fuel-vapor penetration by treating the fuel vapor as particles that exchanged mass, momentum and energy with surrounding. However, in their work they used the molecular viscosity as the criterion to determine how much vapor from the particles is transferred to the gas phase. Gaseous fuel jets have also been modeled by combining Lagrangian particle models and gas jet theory [19].

In this work we extend previous work on grid-independent spray models to include sub-grid scale effects of fuel-vapor mixing. This is achieved by transporting fuel vapor as particles according to turbulent-jet theory. The particles release the fuel vapor mass, momentum and energy once the jet half-width is resolved by the local mesh scale. The results show that accurate predictions of fuel-vapor penetration and flame lift-off length are obtained with coarse mesh resolutions and compare well with results with fine mesh resolutions.

Liquid Spray Model: GASJET model

The liquid spray model of Abani et al. [13] is used that is based on turbulent jet theory, where the air entrainment is modeled as a gas jet of equivalent momentum issuing from the nozzle. The model provides accurate spray tip-penetration and structure with different mesh sizes. The collision model is based on the radius of influence (ROI) approach [15].

In the case of unsteady injections, unsteady turbulent jet theory [16, 17] is used to predict the drop-gas relative velocity. For time-varying injections each droplet responds to a change in injection velocity at the nozzle exit using a time-response derived from Helmholtz vortex theory [16], and an effective injection velocity for each droplet is calculated using Duhamel's superposition principle [16]. These model improvements have been proven to give good predictions of tip penetration for both gasjets and sprays under time-varying injection velocities and different ambient conditions [17].

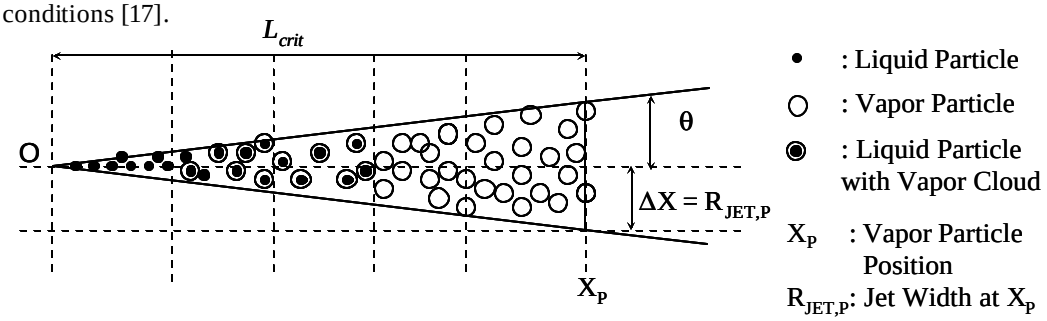

Figure 1: Schematic of the Vapor Particle Method (VPM) for liquid sprays.

Vapor Particle Method: VPM model

For evaporating sprays, the fuel vapor evaporated from a liquid droplet is treated as a Lagrangian vapor particle as depicted in Figure 1. Initially the liquid droplet (black circles in the figure) is injected from the nozzle. Within a short distance the liquid droplet starts evaporating and the evaporated fuel vapor is accumulated in a cloud that travels with the liquid droplet and continues to gain more vapor mass and energy as the liquid droplet evaporates. As long as the parent liquid droplet exists, the fuel vapor cloud continues to travel with the liquid droplet. This is shown in the black and white circles in Figure 1. The liquid droplet continues to be subjected to break-up, collision and coalescence processes. With breakup the vapor cloud continues to be associated with the parent droplet, if there is coalescence, the vapor clouds merge to form one vapor cloud around the new coalesced droplet.

After some distance downstream of the nozzle the liquid droplet completely evaporates and only the vapor cloud remains. At this point the vapor cloud is called a vapor particle, as depicted by the white circles in Figure 1. Transport of the vapor particle continues until the particle reaches a critical distance, L_{crt} from the nozzle that is a function of the numerical mesh size. For a jet half-angle q, L_{crt} is given as:

$$L_{crt} = DX \Big/ \tan\frac{q}{2} \qquad (1)$$

where DX is set equal to the cube root of the cell volume. By this location the vapor cloud and vapor particle transfer their remaining fuel-vapor mass and energy to the gas phase. Prior to reaching L_{crit}, the amount transferred to the gas phase is a fraction of the total fuel vapor mass and energy accumulated in the vapor cloud or vapor particle. . At a time-step n with a computational time-step as Δt, consider the mass of vapor evaporated from the liquid parcel as

$\Delta m_{L,n}$, the mass of vapor received by the computational cell, $\Delta m_{CELL,n}$, then the mass of vapor cloud (or vapor particle), $M_{VP,n}$ associated with the liquid droplet can be solved using following equations.

Mass conservation (i.e., rate of vapor particle radius change):

$$Dm_{CELL,n} = g_n\left(Dm_{L,n} + M_{VP,n-1}\right) = g_n\left(Dm_{L,n} + \sum_{i=1}^{n-1}\left(1-g_i\right)^{n-1} Dm_{L,i}\right) \quad (2)$$

where $M_{VP,n-1} = \sum_{i=1}^{n-1}\left(1-g_i\right)^{n-1} Dm_{L,i}$

and $M_{VP,n-1}$ is the mass of vapor available in the vapor cloud from the previous time-step ($(n-1)^{th}$ time-step). Using Eq. (2), the net mass of vapor left in the vapor particle at the n^{th} time-step then can be found from:

$$\begin{aligned} M_{VP,n} &= \left(1-g_n\right)Dm_{L,n} + \left(1-g_n\right)M_{VP,n-1} \\ &= \left(1-g_n\right)\left[Dm_{L,n} + \sum_{i=1}^{n-1}\left(1-g_i\right)^{n-1} Dm_{L,i}\right] \end{aligned} \quad (3)$$

Momentum conservation (vapor acceleration):

$$m_{VP}\frac{d\vec{\mathbf{V}}_{VP}}{dt} = \mathbf{F}_{D,VP} \quad (4)$$

where $\vec{\mathbf{V}}_{VP}$ are the velocity components of vapor (or gas) particles. $\mathbf{F}_{D,VP}$ is the resistance from the ambient gas which is modeled as a drag force with correlations for a spherical droplet (Amsden, 1997). Similar to the Mass conservation for the vapor particle, the energy conservation (vapor particle internal energy) is expressed as:

$$\text{and} I_{VP,n} = \left(1-g_n\right)\left[DI_{L,n} + \sum_{i=1}^{n-1}\left(1-g_i\right)^{n-1} DI_{L,i}\right] \quad (6)$$

where $I_{VP,n}$ and $\Delta I_{L,n}$ are the internal energy of the vapor particle (or vapor cloud) and the internal energy of the vapor released from the liquid parcel due to evaporation at the n^{th} time-step. The scalar function g_n determines the fraction of the total vapor particle mass and energy (or the total vapor cloud mass and energy) for particle located at position *P*, which is released to the ambient computational cell, respectively, and is given by:

$$g_n = \left(\frac{R_{JET,P}}{DX}\right)^2 \quad (7)$$

This fraction represents the sub-grid vapor particle interactions with the local ambient gas. It is determined by comparing the local jet diffusional length scale (which is the local jet half-width at the particle location) and the local numerical mesh scale, *DX*. $R_{JET,P}$ is the jet width at the location of the particle at position *P*. In this way the scalar function *g* varies as the particle position *P* varies with time and space.

Results and Discussion

1. Evaporating Sprays under non-reacting conditions

The conditions for the non-reacting cases were the constant volume experiments of Naber and Siebers [19] with compressed nitrogen at 1000K, ambient density 58.5kg/m^3, injection pressure 137 MPa and nozzle hole diameter of 257 μm. Five different two-dimensional meshes (0.5° sector mesh) were used with sizes, 4 x 4, 3 x 3, 2 x 2, 1 x 1, 0.5 x 0.5 mm, respectively. For each mesh, the left half of the plots in Figs. 2 and 3 show the gas phase velocity colored with the absolute velocity and over-layed with contours of magnitude 20 and 40 m/s, respectively. The right half of the plot shows the fuel-vapor mass fraction over-layed by contours of magnitude 0.01 and 0.03. The fuel-vapor penetration was determined as the average of location of these two contours.

Figure 2 shows results from the standard KIVA model at 3ms after the start of injection (SOI). For the coarser meshes of 4 x 4 mm and 3 x 3 mm, fuel-vapor penetration is smaller compared to the finer mesh results. The vapor penetration is seen to have converged with the 2 x 2 mm mesh size. Coarser meshes exhibit more numerical diffusion and result in a shorter fuel-vapor penetration. Figure 3 shows the vapor and liquid-tip penetrations with respect to time after SOI. While the liquid penetration seems to agree with the experiment for mesh sizes of 1 and 2 mm, the vapor penetration agrees well only for the finer meshes.

Figure 4 shows the fuel-vapor mass fraction and total velocity for the five mesh sizes for the VPM spray model. The left half also shows blue colored particles that are the vapor particles. In this case the liquid droplets are accompanied by a cloud of fuel vapor which has not yet been transferred to the surrounding gas-phase and travels

with the liquid droplets. As soon as the liquid droplets evaporate completely, the remaining cloud vapor forms the vapor particle. This vapor particle continues to be transported according to jet theory and transfers its fuel-vapor mass, momentum and energy according to Eqs. (2), (3) and (4). The vapor particles exist as long as they remain in the region bounded by the cone angle of the spray, q, and the critical length, L_{crt}.

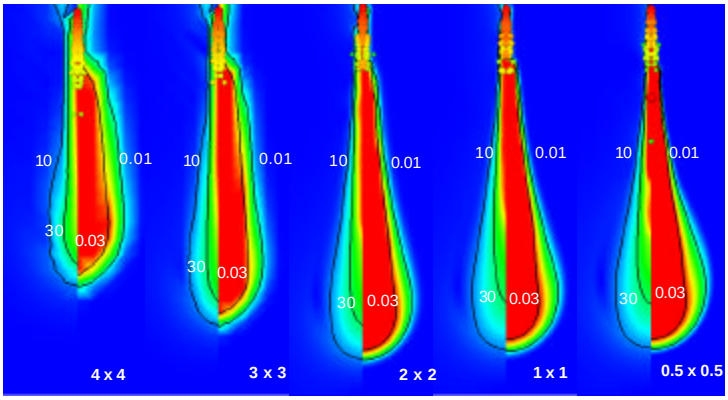

Figure 2. Standard KIVA: Vapor Distribution t= 3ms after SOI. (r_{amb}=58.5 kg/m^3; T_{amb}=1000K)

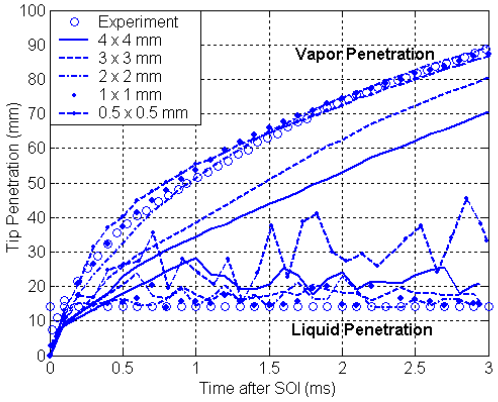

Figure 3. Standard KIVA: Tip Penetration with time. (r_{amb}=58.5 kg/m^3; T_{amb}=1000K)

Figure 5 shows that both the liquid and vapor penetration agree very well with the experiments. This is because the vapor particles penetrate further than the liquid penetration (equal to 14 mm in this case) to L_{crt}=22 mm for the mesh size of 4 x 4 mm. This enables the fuel vapor to penetrate further compared to the standard KIVA model results shown in Figure 3. This avoids the large numerical diffusion in the near-nozzle region of the spray. L_{crt} reduces to 2 mm for the mesh size of 0.5 x 0.5 mm and the VPM model is hardly used.

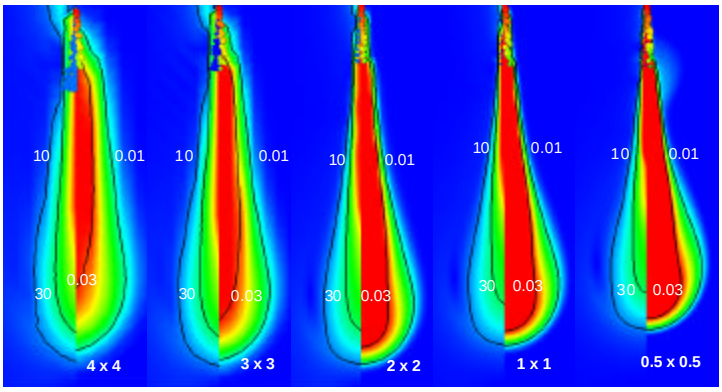

Figure 4. VPM model: Vapor Distribution t= 3ms after SOI. (r_{amb}=58.5 kg/m^3; T_{amb}=1000K)

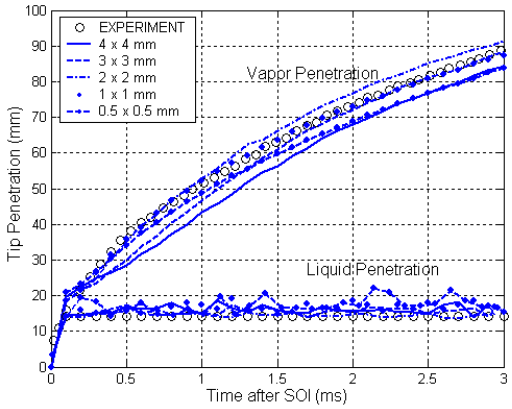

Figure 5. VPM model: Tip Penetration with time. (r_{amb}=58.5 kg/m^3; T_{amb}=1000K)

2. Reacting Sprays:

The conditions for the reacting case are based on the measurements of Picket et al. [21, 22] for sprays in a constant volume chamber with an ambient gas density and temperature of 30 kg/m^3 and 1000K, respectively. The ambient concentrations of O_2, N_2, CO_2 and H_2O are 8, 82, 6.3 and 3.7% mole fraction, respectively. Figure 6 shows the standard KIVA results at t=5.0 ms after SOI for the same 5 meshes described above. The left half of each plot shows the mass fraction of OH in the range 0 to 8e-7. The right half shows the temperature distribution in the range 1000 to 1800 K. Experimentally and in the computations the flame lift-off length was determined based on the location of first OH presence downstream of the nozzle using chemi-luminescence images [21].

Figure 6 shows that for the coarse 4 x 4 mm and 3 x 3 mm meshes, the lift-off length is smaller compared to that obtained using fine meshes. It can also be seen that the liquid penetration length as visualized by the spray particles near the nozzle is also small for coarse mesh cases. Therefore the lift-off length is determined by the fuel-vapor penetration and mixing with the ambient gas and the heat released due to chemical reaction. Both the location of first OH concentration and high temperatures recedes further downstream of the nozzle as the mesh resolution becomes finer. The measured lift-off length was 19.2 mm (white line in Figure 6). The mesh sizes of 2 x 2 mm, 1 x

1 mm and 0.5 x 0.5 mm predictions are close to the measured lift-off length. The coarser 4 x 4 mm and 3 x 3 mm meshes predict smaller-lift off lengths due to the inability of the fuel-vapor to penetrate and mix further downstream.

Figure 7 shows the results from the VPM model. The vapor particles are shown as black colored particles. Because the vapor is transported as particles whose motion is described by jet theory, the vapor-air mixture is able to penetrate further downstream. As compared to the standard KIVA model, there is no accumulation of OH species around the nozzle injector in this case and the presence of OH species appears further downstream close to the measured flame lift-off length. Both the coarser 4 x 4 mm and 3 x 3 mm meshed predict improved flame lift-off length as compared to the standard KIVA model. As the mesh resolution is increased, it can be observed that the lift-off length is predicted consistently and is quite close to the experimental value of 19.2 mm (black line in Figure 7). Note that there are very few vapor particles seen in the fine 0.5 x 0.5 mm mesh because the critical distance L_{crt} is only about 2mm. In addition, the fine mesh result is similar to that of standard KIVA because the liquid penetration is small and the spray behaves as a gaseous jet of fuel-vapor starting a short distance downstream of the nozzle.

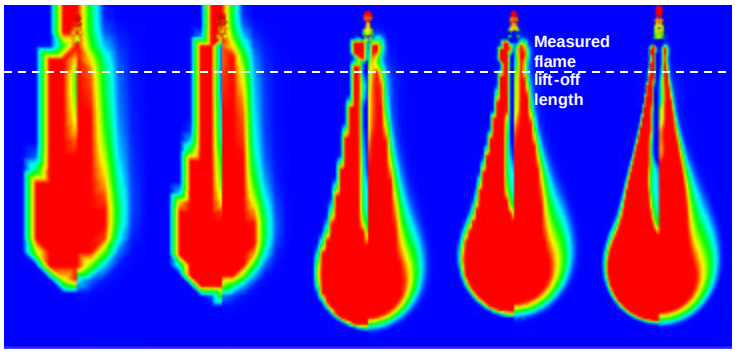

Figure 6. Standard KIVA: Predicted temperature and OH distribution t= 5ms after SOI.

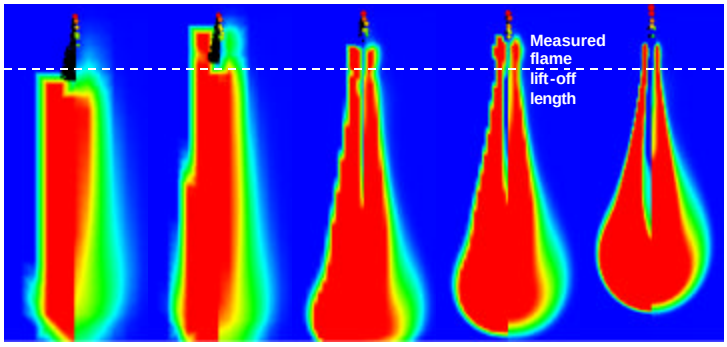

Figure 7. Vapor Particle Method: Predicted temperature and OH distribution t= 5ms after SOI.

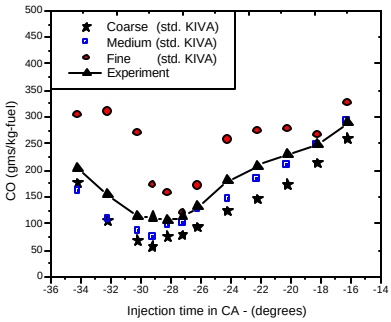

(a) CO emission

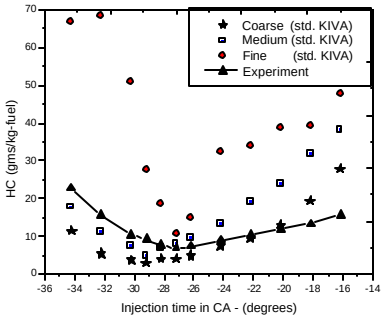

(b) HC emission

Figure 8. Comparison of predicted emissions using standard KIVA.

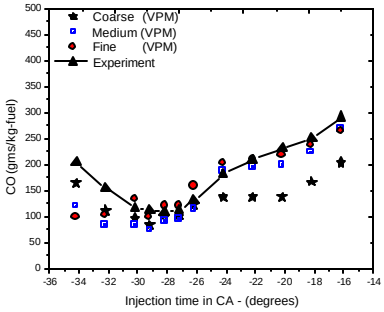

(a) CO emission

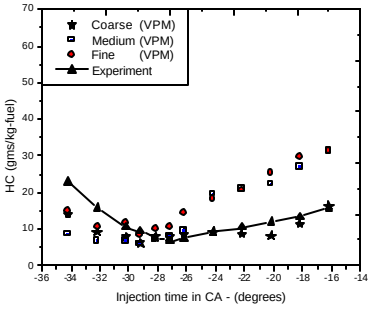

(b) HC emission

Figure 9. Comparison of predicted emissions using VPM spray model.

The VPM model was also used to investigate engine combustion in a 1.9 liter GM engine for different start of injection timings (SOI). Predictions of fuel-vapor distributions were improved using the VPM spray model

compared to the standard KIVA spray model. In addition, emission predictions were found to be fairly grid-independent and agreed well with measurements with the VPM spray model. The computations shown in Figs. 8 and 9 were performed using a 51.4º sector mesh with three different meshes with an average mesh size ranging from 1.3 mm to 4 mm. Figure 8(a) and (b) shows that the predicted CO and HC emissions using the standard KIVA models compare well with measurements for coarse and medium meshes, but not for the finer meshes. Figure 9(a) and (b) shows similar results with the VPM spray model and it is seen that all three meshes give consistent emission predictions and compare well with the measurements. The average computing times for the coarse, medium and fine mesh cases shown in Fig. 9 were 4, 11 and 34 hours, respectively. The computations included the period from intake valve closing (-132º aTDC) to exhaust valve opening (+112º aTDC) and were conducted on an Intel Pentium-4 650 (3.4 GHz). The VPM model contributed negligible additional computer time.

Conclusions

The effect of computational mesh size was investigated for simulations of diesel sprays under both non-reacting and reacting conditions using standard and improved spray models. In the present improved Vapor Particle Method, Lagrangian vapor particles interact with the ambient gas so as to avoid numerical diffusion effects on coarse meshes.

The sub-grid scale turbulent mixing model that transports the vapor as particles improves the results both under non-reacting and reacting conditions. In particular, fuel vapor penetration predictions were improved for coarse numerical meshes. Predicted flame lift-off lengths were also improved for coarse meshes. The improved model also provided grid-independent CO and HC emissions predictions for 1.9 liter GM diesel engine simulations and compared well with measurements. The present VPM model can thus be used as a tool to investigate diesel engine combustion processes on coarse meshes and thereby save computational time. However, future work should include consideration of chemical reactions with the vapor particle approach to improve ignition predictions so as to benefit from the improved predictions of flame lift-off lengths of the present model.

References:

1. Siebers, D. L., and Higgins, B. S, SAE-2001-01-0530, 2001.
2. Siebers, D. L., Higgins, B. S, and Picket, L. M., SAE-2002-01-0890, 2002.
3. Picket, L. M., Siebers, D. L., and Idicheria, C. A., SAE-2005-01-3843, 2005.
4. Vishwanathan, G., and Reitz, R. D., SAE-2008-01-1331.
5. Kokjohn, S. and Reitz, R.D., SAE Paper 2008-01-2412, 2008.
6. Shi, Y., Reitz, R. D., SAE-2008-01-0949, 2008.
7. Duckowicz, J. K., Journal of Computational Physics, Vol. 35, pp. 229-253, 1980.
8. Reitz, R. D., Atomisation and Spray Technology, Vol. 3, pp. 309-337, 1987.
9. Patterson, M.A. and Reitz, R.D., SAE paper 980131, 1998.
10. O'Rourke, P. J., "Collective Drop Effects in Vaporizing Liquid Sprays," Ph. D. thesis 1532 T, Princeton University, August 1981.
11. Abraham, J., SAE paper 970051, 1997.
12. Schmidt, D.P. and Rutland, C.J., Journal of Engineering for Gas Turbines and Power 126, 227-233, 2004.
13. Schlichting, H., Boundary Layer Theory, McGraw-Hill, New York, 1976.
14. Abraham, J., Numerical Heat Transfer, Part-A 30, 347-364, 1996.
15. Abani, N, Munnanur, A., and Reitz, R. D., Journal of Engineering for Gas Turbines and Power, Transactions of the ASME, 130, pp. 032809, 2008.
16. Abani, N., and Reitz, R. D., Physics of. Fluids, 19(12), p125102, December, 2007.
17. Abani, N., Kokjohn, S., Park, S. W., Bergin, M., Munnannur, A., Sun, Y., Ning, W., and Reitz, R. D., SAE-2008-01-0970, 2008.
18. Beard, P., Duclos, J. M., Habchi, C., Bruneaux, G., Mokaddem, K. and Baritaud, T., SAE paper 2000-01-1893, 2000.
19. Hessel, R. P., Abani, N., Aceves, S., and Flowers, D., SAE paper 2006-01-3265, 2006.
20. Naber, J.D., and Siebers, D.L, SAE paper 960034, 1996.
21. Picket, L. M., and Idicheria, C. A., Conference on Thermo-and Fluid Dynamics Processes on Diesel Engines (THIESEL), 2006, Valencia, Spain.
22. http://public.ca.sandia.gov/ecn/cvdata/dsearch.php